Resolving Three Single-Photon Emitters By Only Detecting Third-Order Correlation Functions

Xiao Liang[1,2] and Yong-Sheng Zhang[1,2,*]

[1]*Laboratory of Quantum Information, University of Science and Technology of China, Hefei, 230026, China*
[2]*Synergetic Innovation Center of Quantum Information and Quantum Physics, University of Science and Technology of China, Hefei, 230026, China*

(Dated: October 28, 2016)

Rayleigh criterion has been continuously broken through with modern detecting instruments, many methods on resolving two emitters below the classical diffraction limit has been developed, one of these methods is detecting high order correlation functions of the emitters. We propose a method to resolve the single-photon emitters with only detecting the highest order correlation functions. We find that the variables that characterize the emitters are contained in the highest order correlation functions. Especially when there are more than two emitters, the spatial distribution of the emitters can be deduced only from the highest order correlation functions, which gives a new vision and a new method on beating classical diffraction limit using high order correlation functions.

I. INTRODUCTION

The limited resolution ability of optical imaging is an ancient and crucial problems in many aspects of science. Nearly a century ago, the lowest central distance between two patterns that the light sources can just be resolved is known as the classical diffraction limit or the Rayleigh criterion [1, 2]. One can not distinguish each pattern from the average image when two patterns are overlapped a lot.

Until now, new methods on beating the classical diffraction limit have attracted much attention in both theory [3–12] and experiment [13–21]. In these resolution problems, a common light source is the fluorescence emitter, such as a biological cell [15], single molecule [18], or a nitrogen-vacancy center [19, 20]. Because of the antibunching property of a single-photon emitter [22, 23], in each emission only one photon is emitted. Thus the interval of the emitted photons are much longer than the temporal width of a photon.

The major advantage of single-photon emitter is that the photon number is determinant during each emission process. Therefore when resolving N single-photon emitters, a common used strategy is detecting the high order correlation function of the emitted photons. Because of the single-photon emitters, the N-th order correlation function contains the information up to N emitters. The image of each emitter can be achieved by combining several orders of correlation functions, on the resolved image the width of each emitter can be decreased to $1/\sqrt{N}$ times [13, 19, 20].

Although the resolution ability is not strictly defined, whether the emitters can be resolved or not is intuitional from the image. If the intention of resolution is recovering the diffraction pattern of each emitter, for single-photon emitters the image of each emitter can be reconstructed by combining several orders of correlation functions. This does not require any prior knowledge about the type of the pattern, and the variables describing the emitters are obtainable based on the super resolved image of each emitter [13, 19, 20]. If the intention of resolution ability is obtaining the distance between the emitters, based on Tsang the multi-photon absorption is not necessary. When the emitters can be controlled that there is at most one photon emitted, the estimation error of distance is constant by spatial-mode demultiplexing [9]. In fact, the distance can be obtained via the already reconstructed pattern of each emitter. When resolving single-photon emitters, the total number of the emitters is obtainable by the maximal order of detectable correlation functions. With Gaussian approximations, reconstructing the image of an emitter requires two variables: the width and the central position. The resolution ability is reflected by the relative size of distance and the width of a pattern: $s = d/\sigma$, therefore the image can be reconstructed with the knowledge of s. Above all, if the prior knowledge about the type of the pattern is known, image reconstruction and s-estimation are sufficient to each other.

Besides detecting photon coincide incidence on the same positions, the high order correlation function on different detector positions carries the information about the emitters too [4, 5]. Hence the property of the emitter is achievable without reconstructing the image of each emitter. This can be used when resolving more than two single-photon emitters, since most of the emitted photons are not collected when detecting the correlation function on the same detector positions once a time. Considering the high order correlation functions under all possible detector positions can be used for obtaining the information about the emitters below the classical diffraction limit.

Inspired by these works, we propose a scheme to resolve the single-photon emitters with only the highest order correlation functions in this paper. We find that the distance between the emitters is obtainable from the correlation functions without image reconstruction. Especially when there are more than two emitters, the spatial structure of the emitters is contained in the highest order correlation functions. Therefore, we can resolve the emitters that have complex spatial structures only based on the knowledge of the highest order correlation functions.

This paper is organized as follows: In Sec. II we firstly investigate the resolution of two single-photon emitters with the help of second-order correlation detections using a two-dimensional detector array, we obtain the lowest bound which is approximately half of the classical diffraction limit. In III

* yshzhang@ustc.edu.cn

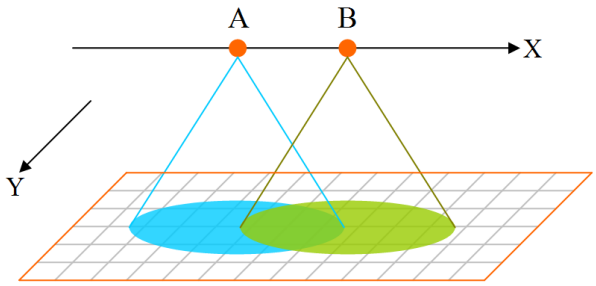

FIG. 1. (Color online) The scheme used for detecting coincide rates in the paper. The two-dimensional detector array is on $X-Y$ plane, the photons emitted from two single-photon emitters trigger two detectors once a time. The PSF of the two emitters are overlapped and their image is obtainable by the average detection intensity formed by the detector array.

we investigate the resolution ability of three collinear single-photon emitters with third-order correlation detections only, we find that the distance between the emitters is the information that can be extracted from the third-order correlation functions under diverse detectors' positions. In IV we further consider the three single-photon emitters are on a two-dimensional plane. We find that by a proper strategy the variables which characterize the spatial structure of the emitters can be obtained by the third-order correlation functions. In V we summarize our work and draw our conclusions.

II. THE BEGINNING: RESOLVING TWO SINGLE-PHOTON EMITTERS

When there are two single-photon emitters, named as A and B, suppose the emitters are too far away that the distance between them can not be directly measured. When the photons arrive at the position of the detectors, they are spreaded with the patterns named as point-spread-functions (PSF). Assuming the PSF of the photons from A and B are Gaussian distributed, and the width of each PSF is known as σ. This is practical, for example σ can be obtained by a nearby separated celestial body on the image. With Gaussian assumption and σ is known, our purpose is to obtain the distance between the emitters, when the magnification ratio of the optical system is known, it is the estimation of the distance between the centrals of the PSF.

Our detection scheme is depicted in Fig.(1), the emitted photons are absorbed by a two-dimensional array of single-photon detectors. On the detectors' array, the PSF of each emitter is two-dimensional, while dimension of X and Y can be written separately. Therefore, in our investigations, dimension Y has no effect on dimension X. Suppose on the plane of the detector-array the PSF from A and B is labeled as: $P_A(x_i)$ and $P_B(x_j)$, where x_i and x_j label the discrete positions of the detectors. Using the Gaussian assumptions, the PSF of each emitter is written as: $P_A(x_i) = \frac{1}{\sqrt{2\pi}\sigma}\exp\left[-\frac{(x+d_1)^2}{2\sigma^2}\right]$,$P_B(x_j) = \frac{1}{\sqrt{2\pi}\sigma}\exp\left[-\frac{(x-d_2)^2}{2\sigma^2}\right]$. Because of the single-photon emitters, the second-order autocorrelation is contributed by the emission of each emitter. Considering the PSF of each emitter, the second order autocorrelation at the detector position $(r_i, r_j)$is:

$$g^{(2)}(r_i, r_j|\tau) = \frac{\langle : I(r_i,\tau)I(r_j,0) : \rangle}{\langle I(r_i,\tau)\rangle\langle I(r_j,0)\rangle}, \tag{1}$$

where the total intensity $I(r_i,\tau) = I_A(r_i,\tau) + I_B(r_i,\tau)$.

Here we are interested in the numerator part of $g^{(2)}$, which is the coincide rate on two detectors at r_i and r_j. Because the photons emitted from A and B are incoherent, in the limit of $\tau \to 0$ the coincide rate at particular two detector position x_i and x_j is:

$$G^{(2)} \propto \eta^2 \left[P_A(x_i)P_B(x_j) + P_A(x_j)P_B(x_i)\right], \tag{2}$$

where η is the detector's single-photon absorption efficiency, it is related to the wavelength of the photon and the type of the detector and it can be previously obtained. Because the Y dimensional of the PSF is integrated to unity, only the X dimensional part of the PSF is considered.

When we have enough number of coincide events, we can divide these events into several parts based on the separation between the two positions that the coincide occurs. On the X-axis direction, we can label the left-sided coincide position as x_i and the right-sided coincide position as x_j. To obtain the coincide number under a certain separation Δ, labeled as $C^{(2)}(\Delta)$, the summation of $G^{(2)}$ under all the positions of x_i which matches $x_j - x_i = \Delta$ is performed, where $\Delta \in [0, +\infty)$. The photons may arrive at the same detector, the detector should have the ability to resolve photon numbers [24]. However our coincide event occurs in the period of τ, when the photons are separated on time scale (such as the constant time difference between the emitters' exitations), the absorbed photons can be resolve by the detector, thus the coincide event on the same detector can be observed. To reveal the relation between Δ and the total distance d_1+d_2, $C^{(2)}(\Delta)$ can be obtained by integrating x_i from $-\infty$ to $+\infty$:

$$C^{(2)}(\Delta) \propto \eta^2 \left[\exp\left(\frac{\Delta d_2}{\sigma^2}\right) + \exp\left(\frac{\Delta d_1}{\sigma^2}\right)\right] e^{\frac{-(2\Delta+d_1-d_2)^2}{16\sigma^2}}. \tag{3}$$

Now we have a new distribution respect to detector separation: Δ, since enough coincide events are collected by the detector array, the possibility of $C^{(2)}(\Delta)$ is relative to the summation of $C^{(2)}$ under all possible Δ values, thus we have the normalized distribution of coincide rate under the separation:

$$c^{(2)}(\Delta) = C^2(\Delta) / \sum_{\Delta=0}^{+\infty} C^{(2)}(\Delta). \tag{4}$$

The maximal point of $c^{(2)}$ is obtainable by investigating the first derivative of $C^{(2)}(\Delta)$, using Eq.(3) we have the requirement of Δ:

$$\frac{\Delta}{d_1+d_2} = \tanh\left[(d_1+d_2)\frac{\Delta}{2\sigma^2}\right]. \tag{5}$$

It can be further veryfied that when Eq.(5) holds the corre-

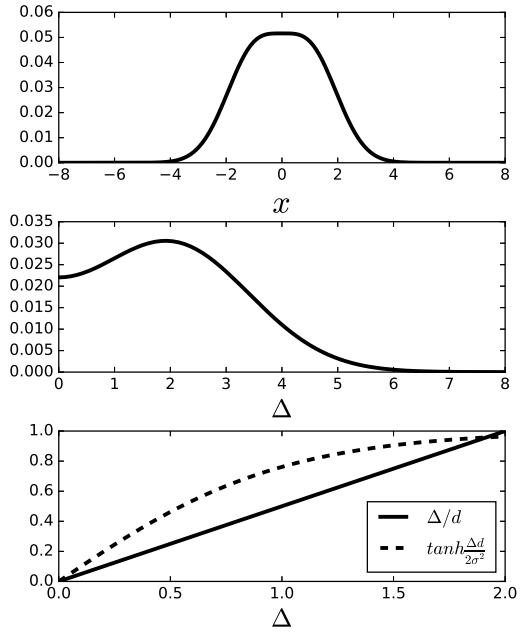

FIG. 2. (Color online) The upper figure reveals the image of two single-photon emitters with $\sigma = 1$ and $d = 2$. The middle figure reveals the distribution of coincide events $c^{(2)}(\Delta)$ based on Eq.(3) and Eq.(4). The lower figure reveals the left side and the right side of the equality in Eq.(5), the intersection is where the peak of $c^{(2)}$ occurs.

sponding value of c^2 is the peak value. Therefore we have the relationship between separation Δ and the distance between the emitters $d_1 + d_2$ at the peak value of coincide rate distribution. The distance between the emitters can be obtained by finding the peak value of $c^{(2)}$. Usually $\Delta = 0$ is not our interested point, therefore whether the coincide event can be observed by one detector or not is not crucial in our strategy. It is revealed from Eq.(5) the peak value of $c^{(2)}$ does not depend on the relative position of the reference point, it only depends on the total distance $d_1 + d_2$, therefore compared to first order detections, using second-order coincides can avoid the extra error introduced by mis-alignment.

To demonstrate the power of coincide detection, a comparison between direct image and coincide rate observations is depicted in Fig.(2), while the upper figure reveals the direct image and the middle figure reveals the function of $c^{(2)}(\Delta)$. With σ is known, in principle, the emitters' distance is obtainable if there exists a peak in $c^{(2)}(\Delta)$ in the range of $\Delta \in (0, +\infty)$. As revealed by Eq.(6) and the lower figure in Fig.(2), the left side and the right side of the equality are both monotonic function with respect to Δ. To ensure the existence of peak value, at $\Delta = 0$ the first derivative of the right side should be greater than the left side, thus we have the lowest bound that the distance can be obtained:

$$d > \sqrt{2}\sigma, \tag{6}$$

this is obviously lower than Rayleigh criterion. Using the Gaussian assumption the Rayleigh criterion is approximately 3σ, the coincide detection can reduce the bound to approximately half of the Rayleigh criterion.

III. RESOLVING THREE COLLINEAR SINGLE-PHOTON EMITTERS

In this section we investigate the resolution ability of three collinear emitters using the triple-photon coincide rates detected by a two-dimensional detector array, our scheme is similar to that depicted in Fig.(1) except there are three emitters on the axis of X. We label the emitters as A, B and C, and the distance between A and B: d_1, B and C: d_2. Thus the PSF of each emitter can be written as: $P_A(x,y) = \frac{1}{2\pi\sigma^2}\exp\left[-\frac{(x+\lambda+d_1)^2+y^2}{2\sigma^2}\right]$, $P_B(x,y) = \frac{1}{2\pi\sigma^2}\exp\left[-\frac{(x+\lambda)^2+y^2}{2\sigma^2}\right]$, $P_C(x,y) = \frac{1}{2\pi\sigma^2}\exp\left[-\frac{(x+\lambda-d_2)^2+y^2}{2\sigma^2}\right]$, where λ is the alignment parameter. The third-order autocorrelation at the detectors' position (r_i, r_j, r_k) is:

$$g^{(3)}(r_i, r_j, r_k|\tau_1, \tau_2) = \frac{\langle : I(r_i,\tau_1)I(r_j,\tau_2)I(r_k,0) : \rangle}{\langle I(r_i,\tau_1)\rangle\langle I(r_j,\tau_2)\rangle\langle I(r_k,0)\rangle}, \tag{7}$$

where the total intensity at time τ is $I(r,\tau) = I_A(r,\tau) + I_B(r,\tau) + I_C(r,\tau)$.

We are interested in the numerator part of $g^{(3)}$, which is the triple-photon coincide rates where the photons arrive at the detector array are: r_i, r_j and r_k. Because the Y dimensional part of the PSF is integrated to unity, our investigateion can be simplified on dimension X only. Therefore in the limit of $\tau_{1,2} \to 0$, at x_i, x_j and x_k the triple-photon coincide rate can be written as:

$$\begin{aligned} G^{(3)}/\eta^3 \propto & P_A(x_i)\left[P_B(x_j)P_C(x_k) + P_B(x_k)P_C(x_j)\right] + \\ & P_A(x_j)\left[P_B(x_i)P_C(x_k) + P_B(x_k)P_C(x_i)\right] + \\ & P_A(x_k)\left[P_B(x_i)P_C(x_j) + P_B(x_j)P_C(x_i)\right]. \end{aligned} \tag{8}$$

When enough samples are collected, we can divide the coincide event based on the separations between x_i, x_j and x_k, for three points at least two separations are needed, named as δ_1 and δ_2 where $\delta_{1,2} \in [0, +\infty)$. Since i, j and k are just labels for coincide positions, relative to X-axis direction we label x_i as the left-sided position x_j as the middle position and x_k as the right-sided position, therefore $\delta_{1,2}$ can be defined as $\delta_1 = x_j - x_i$, $\delta_2 = x_k - x_j$. To obtain the coincide numbers under a given $\delta_{1,2}$, a summation under all possible positions of x_i is performed. For the purpose of simplicity, we firstly investigate the formation of coincide rate under $\sigma = 1$, $d_1 = d_2 = d$ and $\lambda = 0$, after integrating on all possible x_i values we have the formation of coincide rate, $C^{(3)}(\delta_1, \delta_2)$:

$$\begin{aligned} C^{(3)}(\delta_1,\delta_2)/\eta^3 \propto & [e^{d(\delta_1+\delta_2)} + e^{3d(\delta_1+\delta_2)} + e^{d(\delta_1+2\delta_2)} + \\ & e^{d(2\delta_1+\delta_2)} + e^{d(2\delta_1+3\delta_2)} + e^{d(3\delta_1+2\delta_2)}] \\ & e^{-d^2-2d\delta_1-2d\delta_2-\delta_1^2/3-\delta_1\delta_2/3-\delta_2^2/3}. \end{aligned} \tag{9}$$

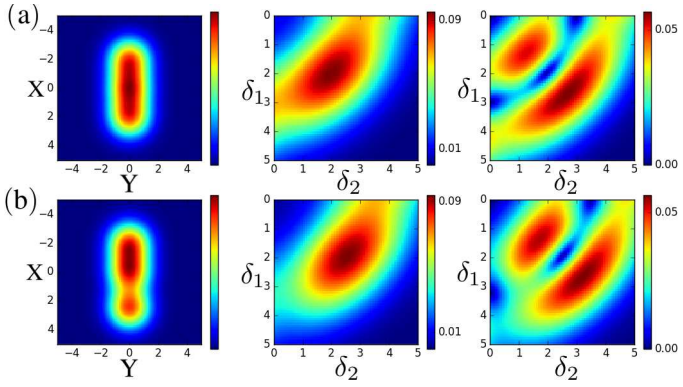

FIG. 3. (Color online) The resolution ability of three collinear emitters with the help of third-order correlation distributions. (a) From left to right, the first figure is the image of three emitters with $d = 2$, while the mis-alignment parameter $\lambda = 0$. The second figure reveals the coincide rate $C^{(3)}(\delta_1, \delta_2)$ based on Eq.(9). The third figure reveals the function of $f(\delta_1, \delta_2)$. (b) From left to right, the first, the second and the third figure reveal the image, the $C^{(3)}(\delta_1, \delta_2)$ and the $f(\delta_1, \delta_2)$, respectively. With the distance between A and B: $d_1 = 2$, B and C: $d_2 = 2.5$, under $\lambda = 0$.

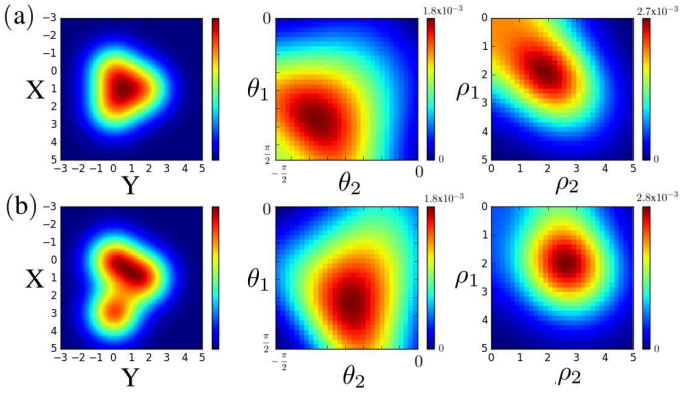

FIG. 4. (Color online) The resolution ability of three emitters on a two-dimensional plane. The difference in the arrangements of the emitters is revealed in the context in IV. In both Row (a) and Rwo (b), from left to right, the first figure is the image of three emitters. The second figure is the normalized distribution of $D^{(3)}(\theta_1, \theta_2)$ as revealed by Eq.(12). The third figure is the distribution of coincide rate with respect to separations under the optimal values of angles.

Now we have a new distribution with respect to δ_1 and δ_2, with enough collecting samples we can normalize $C^{(3)}$ on all possible variables of (δ_1, δ_2), thus we have the normalized distribution of $C^{(3)}(\delta_1, \delta_2)$:

$$c^{(3)}(\delta_1, \delta_2) = C^{(3)}(\delta_1, \delta_2) / \sum_{\delta_1, \delta_2 = 0}^{+\infty} C^{(3)}(\delta_1, \delta_2). \qquad (10)$$

To find out the maximal position of $c^{(3)}$ we can evaluate the function: $f(\delta_1, \delta_2) = \sqrt{\sum_{k=1,2} (\frac{\partial C^{(3)}}{\partial \delta_k})^2}$, the values of (δ_1, δ_2) on the zero point of $f(\delta_1, \delta_2)$ is the candidate position for the peak of $C^{(3)}(\delta_1, \delta_2)$. In fact, the coincide rate obtained by Eq.(9) and Eq.(10) is only related to the relative separation: δ_1 and δ_2, namely, if all the spatial position that has non-zero photon absorption are considered, changing the relative position between the PSF and the reference point makes no difference to $C^{(3)}$, therefore for simplicity we set $\lambda = 0$.

Here, we numerically investigate the resolution ability of emitter A, B and C based on $C^{(3)}(\delta_1, \delta_2)$ and $f(\delta_1, \delta_2)$. Firstly we investigate the distance between A and B. B and C is the same that $d = 2$. In Row (a) of Fig.(3), the spatial image of the PSF is depicted by the left-sided figure, obviously it is difficult (or not possible) to distinguish the PSF of each emitter by directly observing the image. The middle figure depicts the normalized coincide rate with variable of δ_1 and δ_2, to determine the corresponding values of $\delta_{1,2}$ for the peak, the function of $f(\delta_1, \delta_2)$ is numberically depicted in the right-sided figure. The investigation of $f(\delta_1, \delta_2)$ is useful for error estimation, because the distance is obtainable from the distinct peak of coincide distribution. It is revealed by the right-sided figure that the maximum of $c^{(3)}$ occurs in a small range of $\delta_{1,2}$ where $f(\delta_1, \delta_2) \approx 0$. At the central of the peak there is $\delta_1 = \delta 2 \approx 2$, which is very close to the distance: d.

In the situation depicted in Row (a) of Fig.(3), because the distance between A and B, B and C is the same, there is only one variable to be estimated: d. When the emitters are not placed homogeneously, for example the distances between A and B, B and C are d_1 and d_2, we have $d_1 \neq d_2$. There are two variables to be estimated, as depicted in Row (b) of Fig.(3) we show that the information of d_1 and d_2 is contained in the distribution of $C^{(3)}(\delta_1, \delta_2)$, the values of $d_{1,2}$ can be obtained by investigating the peak of $C^{(3)}(\delta_1, \delta_2)$ too. Since the distance is obtained via the distribution of $C^{(3)}$ under enough detected samples, with the knowledge of the shape of $C^{(3)}$ and $f(\delta_1, \delta_2)$ the distance can be obtained precisely via the relationship between $d_{1,2}$ and $\delta_{1,2}$. The estimation ability of distance is related to whether the peak of $C^{(3)}$ is distinct or not, if the emitters are too close that the peak of $C^{(3)}$ is implicit or the peak does not exist, the estimation ability is low or the distance is unobtainable.

As depicted by the numerical result in Row (b) of Fig.(3), when $d_1 = 2$ and $d_2 = 2.5$ the PSF of each emitter can hardly be resolved from the average image, as the revealed by left-sided figure. Combining the middle and the right-sided figures, the corresponding values of $\delta_{1,2}$ to the peak of $C^{(3)}$ is $\delta_1 \approx 2$ and $\delta_2 \approx 2.5$. These results reflect that the distance values can be estimated by the optimal δ_1 and δ_2 which corresponds to the peak position of the coincide distribution. Although the estimation may be biased when $d_{1,2}$ is too small (like the situation with two emitters), because the peak position is determined by the zero-point of $f(\delta_1, \delta_2)$ and the relationship between $d_{1,2}$ and $\delta_{1,2}$ can be complicated, however it still gives approximated values of $d_{1,2}$ under $d_{1,2} \geq 2$, which is the capability that can not be provided by the average image alone.

IV. RESOLVING THREE SINGLE-PHOTON EMITTERS ON TWO DIMENSIONS

In the previous section, we showed the enhanced resolution ability of three collinear emitters by third-order correlation detections. In reality the three emitters can be placed on a two-dimensional plane, the relative positions of the emitters is related to not only distances but also angles. Therefore, to resolve the emitters on two-dimensional plane by third-order correlations, the distances between the triggered detectors are represented by two-dimensional vectors.

Here we still use the two-dimensional detector array depicted in Fig.(1) to perform the third-order correlation detections, while the formation of $g^{(3)}$ is expressed by Eq.(7), with the separations between $r_{i,j,k}$ described by two-dimensional vectors, the triple-photon coincide rate is described by Eq.(8)

The total third-order coincide events is divided based on the relative positions between the triggered detectors. For example, when the triggered detectors are at positions $\vec{r}_{i,j,k} = (x_{i,j,k}, y_{i,j,k})$, the distances between i, j and j, k can be expressed by two vector: (ρ_1, θ_1) and (ρ_2, θ_2):

$$x_j = x_i + \rho_1 \cos(\theta_1),\ y_j = y_i + \rho_1 \sin(\theta_1), \tag{11a}$$

$$x_k = x_j + \rho_2 \cos(\theta_2),\ y_k = y_j + \rho_2 \sin(\theta_2), \tag{11b}$$

where $\rho_{1,2} \in [0, +\infty)$ and $\theta_{1,2} \in [-\pi/2, \pi/2)$ for covering all possible events under the integration on (x_i, y_i).

For the purpose of high measuring precision, the size of each detector in the detector array should not be too large. Therefore $\rho_{1,2}$, $\theta_{1,2}$ and (x_i, y_i) can be considered as continuous variables. As $c^{(3)}$ has four variables, finding the four optimal variables simultaneously is too computational costly. Hence we firstly try to find out the optimal angles under all possible distance values, then continue to find out the optimal separations based on the knowledge of optimal angles.

In our numerical simulations we investigate two kinds of the emitters' arrangements. The first kind is when the emitters are on the vertexes of an equilateral triangle, since the function of $C^{(3)}$ is obtained after integrating $G^{(3)}$ on all possible detector positions, we can write the PSF of each emitter as: $P_A(x, y) = \frac{1}{2\pi\sigma^2}\exp\left[-\frac{x^2+y^2}{2\sigma^2}\right]$, $P_C(x, y) = \frac{1}{2\pi\sigma^2}\exp\left[-\frac{(x-r)^2+y^2}{2\sigma^2}\right]$, $P_B(x, y) = \frac{1}{2\pi\sigma^2}\exp\left[-\frac{(x-r/2)^2+(y-\sqrt{3}r/2)^2}{2\sigma^2}\right]$, where r is the side length of the triangle, we assume $r = 2$ and $\sigma = 1$ in our numerical investigations. In this case, after considering all the possible positions on the detector array and all the possible separation values of (ρ_1, ρ_2), we obtain a distribution with respect to only the angles (θ_1, θ_2), this process can be expressed as:

$$D^{(3)}(\theta_1, \theta_2) = \sum_{\rho_1, \rho_2 = 0}^{+\infty} C^{(3)}(\rho_1, \rho_2, \theta_1, \theta_2), \tag{12}$$

with continuous variable assumptions the summations on (ρ_1, ρ_2) can be replaced as integrations. The physical meaning of $D^{(3)}(\theta_1, \theta_2)$ is the possibility of finding the vectors with (θ_1, θ_2) under all possible detector positions and all possible separations of (ρ_1, ρ_2), such distribution is achievable when enough samples of third-order correlations are collected. The normalized distribution of $D^{(3)}(\theta_1, \theta_2)$ is depicted in the middle figure in Row (a) of Fig.(4). The optimal value of (θ_1, θ_2) is approximately $(0.35\pi, -0.35\pi)$, which is close to the real value that $(\pi/3, -\pi/3)$ with 6% estimation error. Under the optimal angles, the distribution with respect to (ρ_1, ρ_2) under the integration on (x_i, y_i) can be investigated, as the right-sided figure in Row (b) of Fig.(4) depicts. Clearly, the distance between emitter A and C, C and B can be obtained by the optimal values of $\rho_1 = \rho_2 \approx 2.00$. Compared to the average image depicted by the left-sided figure in Row (a) of Fig.(4), the emitters are too close that only one light spot is observed.

The second kind of the emitters arrangement is when one of the emitters is arranged further: $P_C(x, y) = \frac{1}{2\pi\sigma^2}\exp\left[-\frac{(x-1.5r)^2+y^2}{2\sigma^2}\right]$, while the average image is depicted by the left-sided figure in Row (b) of Fig.(4). As revealed by the middle and the right-sided figure, the optimal angle of θ_2 becomes smaller and the optimal distance of ρ_2 becomes larger. The optimal values obtained from the peaks of the middle figure and the right-sided figure are: $(\theta_1 \approx 0.33\pi, \theta_2 \approx 0.23\pi)$ and $(\rho_1 \approx 2.00, \rho_2 \approx 2.64)$, which is very close the real values based on the arrangement of the emitters.

In the above numerical investigations, we assume that the separation between the emitters are twice as the width of the approximated Gaussian distribution: $d/\sigma = 2$. The resolving capability of high order correlation detections require $s = d/\sigma$ is not too small, for example with only two emitters s should be greater than $\sqrt{2}$. When a third emitter is introduced, since the resolution capability depends on whether the optimal values exist, the critical distance is depend on how the emitters are arranged on the two-dimensional plane. From the numerical results depicted in Fig.(4), the variables that characterize the structure of the emitters can be achieved by only detecting the third-order correlation functions with $s = 2$.

V. SUMMARY AND CONCLUSIONS

In this paper, we propose that the information of the emitters is obtained by the highest order of correlation functions, while the emitters can not be resolved from the image of the first-order correlation function.

In our investigations, the variables that characterize the emitters is not based on a direct measurement, they are based on the final distribution of high order correlations when enough samples of correlation functions are collected. Thus the variables such as distance or angles of the emitters are indirectly obtained by the optimal values which characterize the distributions. Unlike two emitters that the relationship revealed by Eq.(5) is obtained analytically, for three emitters the relationship between the optimal values and the real values which describe the emitters is determined by the actual arrangement of the emitters, which is not the prior knowledge.

Therefore, the estimation error is the estimation bias based on the relationship between the distribution's peak and the variables that characterize the distribution.

Compared to detect high order correlation functions on the same position, the correlation functions on various detector positions can be detected using a two-dimensional detector array. For precisely obtaining the high order distributions, the number of the detectors is not limited. Therefore enormous data samples should be collected, during the collecting process, a computer program should be used to classify each detection based on the relative positions of the triggered detectors, such classification criteria should cover all the possible measuring outcomes without duplications.

The advantage of using detector array is that the high order correlations on different positions can be detected, which gives clues about the emitters without reconstructing the image of each emitter. This is useful especially when there are several single-photon emitters located in a small area, since reconstructing the image of each emitter is based on the correlation function on the same position, using a two-dimensional detector array is more efficient for photon collections.

In conclusion, we conclude that three single-photon emitters can be resolved by only detecting third-order correlation functions. The variables that characterize the emitters' spatial distribution is obtainable by finding the optimal positions from the distributions of third-order correlation functions. The only reconstructed image is the distribution of third-order correlation function, and no post-processing of the collected data is performed.

ACKNOWLEDGMENTS

This work is funded by National Natural Science Foundation of China (No. 61275122, 11674306, 61590932), the Innovation Funds and Strategic Priority Research Program (B) of CAS (No. XDB01030200), and the National Key R&D Program (No. 2016YFA0301700).

[1] M. Born, E. Wolf,"Principles of optics: electromagnetic theory of propagation, interference and diffraction of light," (Cambridge University Press, Cambridge, 1999).

[2] Lord Rayleigh. XXXI. "Investigations in optics, with special reference to the spectroscope." The London, Edinburgh, and Dublin Philosophical Magazine and Journal of Science **8**, 261-274 (1879).

[3] O. Schwartz and D. Oron, "Improved resolution in fluorescence microscopy using quantum correlations," Phys. Rev. A **85**, 033812 (2012).

[4] M. E. Pearce, T. Mehringer, J. von Zanthier and P. Kok, "Precision estimation of source dimensions from higher-order intensity correlations." Phys. Rev. A **92** 043831 (2015).

[5] Hong-Chao Liu, "High-order Correlation of Chaotic Bosons and Fermions," Phys. Rev. A **94** 023827 (2016).

[6] M. Tsang, R. Nair and X. M. Lu, "Quantum theory of superresolution for two incoherent optical point sources," Phys. Rev. X **6** 031033 (2016).

[7] A. N. Boto, P. Kok, D. S. Abrams, S. L. Braunstein, C. P. Williams and J. P. Dowling, "Quantum Interferometric Optical Lithography: Exploiting Entanglement to Beat the Diffraction Limit," Phys. Rev. Lett. **85**, 2733 (2000).

[8] C. A. Pérez-Delgado, M. E. Pearce and P. Kok, "Fundamental Limits of Classical and Quantum Imaging," Phys. Rev. Lett. **109**, 123601 (2012).

[9] M. Tsang, "Quantum Imaging Beyond the Diffraction Limit by Optical Centroid Measurements," Phys. Rev. Lett. **102** 253601 (2009).

[10] M. Tsang, "Relationshop Between Resolution Enhancement And Multiphoton Absorption in Quantum Lithography", Phys. Rev. A **75** 043813 (2007).

[11] K. Lyons, S. Pang, P. G. Kwiat and A. N. Jordan, "Precision Optical Displacement Measurements Using Biphotons," Phys. Rev. A **93** 043841 (2016).

[12] S. W. Hell and J. Wichmann, "Breaking the diffraction resolution limit by stimulated emission: stimulated-emission-depletion fluorescence microscopy." Opt. Lett. **19**, 780-782 (1994).

[13] O. Schwartz, J. M. Levitt, R. Tenne, S. Itzhakov, Z. Deutsch and D. Oron, "Superresolution Microscopy with Quantum Emitters," Nano. Lett. **13** 5832-5836 (2013).

[14] M. A. Taylor, J. Janousek, V. Daria, J. Knittel, B. Hage, H. Bachor and W. P. Bowen, "Biological Measurement Beyond the Quantum Limit," Nature Photonics **7** 229-233 (2013).

[15] M. Fernandez-Suarez and A. Y. Ting, "Fluorescent Probes For Super-resolution Imaging in Living Cells," Nat. Rev. Mol. Cell. Biol. **9** 929-943 (2008).

[16] V. Giovannetti, S. Lloyd, L. Maccone and J. H. Shapiro, "Sub-Rayleigh-diffraction-bound Quantum Imaging," Phys. Rev. A **79**, 013827 (2009).

[17] S. Oppel, T. B uttner, P. Kok and J. von Zanthier, "Superresolving multiphoton interferences with independent light sources." Phys. Rev. Lett. **109**, 233603 (2012).

[18] S. Ram, E. S. Ward and R. J. Ober, "Beyond Rayleigh's Criterion: A Resolution Measure with Application to Single-molecule Microscopy," Proc. Natl. Acad. Sci. U.S.A. **103** 4457-4462 (2006).

[19] J. M. Cui, F. W. Sun, X. D. Chen, Z. J. Gong and G. C. Guo, "Quantum Statistical Imaging of Particles without Restriction of the Diffraction Limit," Phys. Rev. Lett. **110**, 153901 (2013).

[20] D. G. Monticone, K. Katamadze, P. Traina, E. Moreva, J. Forneris, I. Ruo-Berchera, P. Olivero, I. P. Degiovanni, G. Brida and M. Genovese, "Beating the Abbe Diffraction Limit in Confocal Microscopy via Nonclassical Photon Statistics," Phys. Rev. Lett. **113**, 143602 (2014).

[21] S. W. Hell, "Far-field optical nanoscopy," Science **316**, 1153-1158 (2007).

[22] C. Kurtsiefer, S. Mayer, P. Zarda and H. Weinfurter, "Stable Solid-State Source of Single Photons," Phys. Rev. Lett. **85** 2 (2000).

[23] M. Berthel, O. Mollet, G. Dantelle, T. Gacoin, S. Huant and A. Drezet, "Photophysics of Single Nitrogen-Vacancy Centers in Diamond Nanocrystals," Phys. Rev. B **91** 035308 (2015).

[24] R. H. Hadfield, "Single-Photon Detectors for Optical Information Applications," Nature Photon. **3** 696-705 (2009).